10.1098/rsta.2003.1170

THE ROYAL SOCIETY

Solid–solid contacts due to surface roughness and their effects on suspension behaviour

By Robert H. Davis[1], Yu Zhao[2], Kevin P. Galvin[2] and Helen J. Wilson[3]

[1]*University of Colorado, Boulder, CO 80309-0424, USA* (robert.davis@colorado.edu)

[2]*Department of Chemical Engineering, University of Newcastle, Callaghan, NSW 2308, Australia*

[3]*Department of Applied Mathematics, University of Leeds, Woodhouse Lane, Leeds LS2 9JT, UK*

Published online 26 March 2003

Solid–solid contacts due to microscopic surface roughness in viscous fluids were examined by observing the translational and rotational behaviours of a suspended sphere falling past a lighter sphere or down an inclined surface. In both cases, a roll–slip behaviour was observed, with the gravitational forces balanced by not only hydrodynamic forces but also normal and tangential solid–solid contact forces. Moreover, the nominal separation between the surfaces due to microscopic surface roughness elements is not constant but instead varies due to multiple roughness scales. By inverting the system, so that the heavy sphere fell away from the lighter sphere or the plane, it was found that the average nominal separation increases with increasing angle of inclination of the plane or the surface of the lighter sphere from horizontal; the larger asperities lift the sphere up from the opposing surface and then gravity at large angles of inclination is too weak to pull the sphere back down to the opposing surface before another large asperity is encountered.

The existence of microscopic surface roughness and solid–solid contacts is shown to modify the rheological properties of suspensions. For example, the presence of compressive, but not tensile, contact forces removes the reversibility of sphere–sphere interactions and breaks the symmetry of the particle trajectories. As a result, suspensions of rough spheres exhibit normal stress differences that are absent for smooth spheres. For the conditions studied, surface roughness reduces the effective viscosity of a suspension by limiting the lubrication resistance during near-contact motion, and it also modifies the suspension microstructure and hydrodynamic diffusivity.

Keywords: suspensions; hydrodynamic interactions; friction; small Reynolds number; rheology

1. Introduction

Suspensions are comprised of small solid particles suspended in a liquid. They are found in natural phenomena such as blood flow and sediment transport, and also in industrial processes such as fluidization and filtration.

One contribution of 12 to a Theme 'Micromechanics of fluid suspensions and solid composites'.

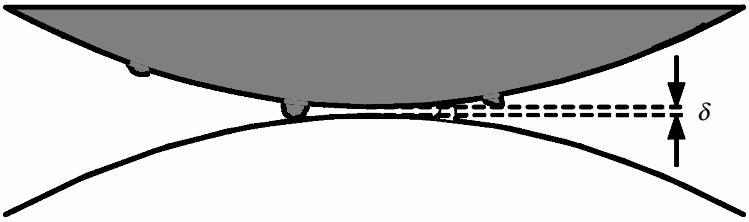

Figure 1. Schematic of contact between two particles due to microscopic surface roughness; δ is the separation between the nominal surfaces.

In previous models of suspension behaviour, it was commonly assumed that the surrounding fluid acts as a lubricant to prevent direct solid–solid contacts between the surfaces of the neighbouring particles. While this assumption may be valid for particles with smooth surfaces, recent research has revealed that microscopic roughness elements on the particle surfaces allow for solid–solid contacts (see figure 1) and consequently modify the suspension behaviour. For example, Parsi & Gadala-Maria (1987) showed that the pair-distribution function for sheared suspensions has different values on the approaching and receding sides of a reference sphere, which violates the symmetry predicted for smooth spheres based on the linearity and reversibility of the creeping flow equations. This finding was verified by Rampall *et al.* (1997), who showed that their measurements of the pair-distribution function in dilute suspensions are consistent with a simple model that includes particle surface roughness and irreversible solid–solid contacts. The irreversibility occurs because the contacts allow for a compressive force that stops the relative motion along the line of centres in the fore region of shear, where the particles are pushed together, but not a tensile force that would prevent the particles from separating in the aft region, where the shear flow acts to pull the particles apart. Further evidence of particle–particle contacts was provided by Tabatabaian & Cox (1991) and Zeng *et al.* (1996), who showed that the symmetry of the trajectories predicted for two smooth spheres interacting in shear flow (see figure 2) and gravity sedimentation, respectively, is broken for rough spheres due to the occurrence of irreversible contacts.

Smart & Leighton (1989) used scanning electron micrographs and hydrodynamic methods to show that particles which appear to be smooth to the naked eye or when touched may have microscopic roughness elements on their surfaces, which are typically of order 10^{-3}–10^{-2} times the particle radii. Davis (1992) and daCunha & Hinch (1996) showed that these roughness heights are sufficient to break the symmetry of the trajectories expected for smooth particles and to cause or modify hydrodynamic diffusion in dilute suspensions undergoing sedimentation or shear (see figure 3), respectively. More recently, Wilson & Davis (2000, 2002) performed theoretical and simulation work to predict how microscopic surface roughness and particle–particle contacts modify the effective viscosity of suspensions and lead to normal stress differences that are absent for suspensions of smooth spheres. In the related field of tribology, it is well known (e.g. Persson 1998) that microscopic surface roughness and solid–solid contacts can affect the frictional and lubrication interactions of two solid surfaces sliding over each other with a thin intervening layer of a viscous fluid.

In the present paper, we review and expand recent work that our group has performed to elucidate the nature of direct particle–particle or particle–surface contacts

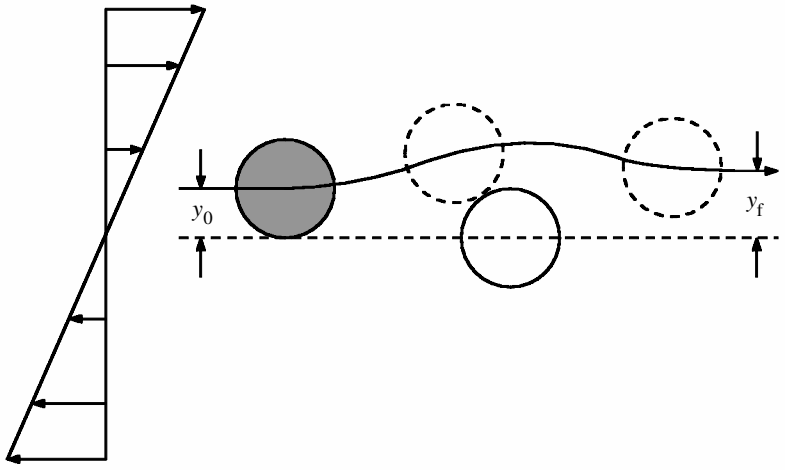

Figure 2. Trajectory of one sphere (shaded initial position) relative to a second sphere in simple shear flow. The two solid spheres come into contact on microscopic roughness elements, which breaks the fore-and-aft symmetry of the trajectory so that the final offset, y_f, in the direction of the velocity gradient is greater than the initial offset, y_0.

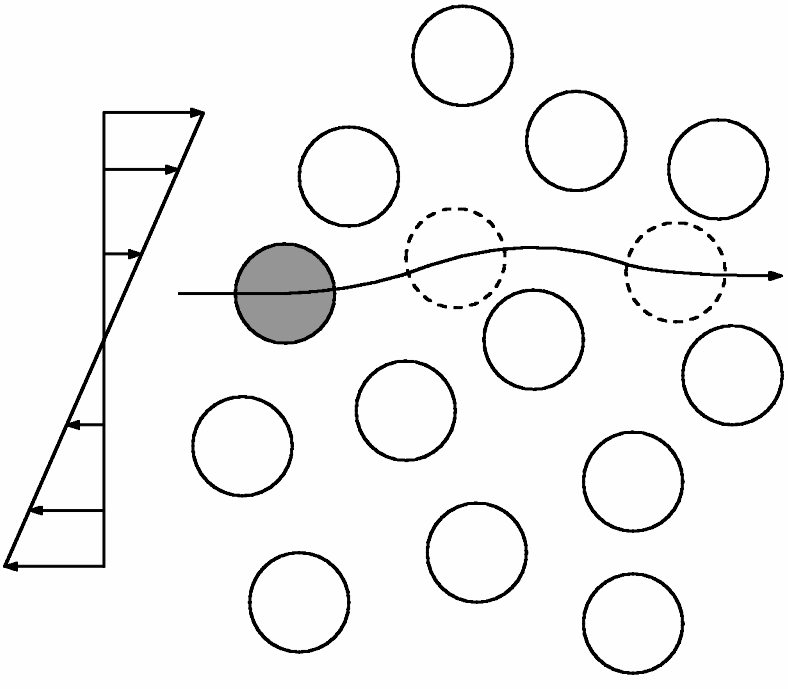

Figure 3. Trajectory of a test sphere (shaded initial position) in a dilute suspension of spherical particles subject to simple shear flow. The test sphere undergoes a wandering motion about the time-averaged streamline through its initial position, due to hydrodynamic interactions with the other particles, giving rise to hydrodynamic diffusion. This motion is affected by the presence of irreversible particle contacts due to microscopic surface roughness.

in a viscous fluid, and also we describe some of the effects that these contacts have on suspension behaviour. In § 2, the idealized problem of a sphere moving due to gravity down an inclined plane is examined to provide models and understanding of the combined effects of hydrodynamic forces and solid–mechanic forces on resisting and governing the particle motion. These concepts are extended in § 3 to the more complicated problem of a heavy sphere sedimenting past a light sphere in a viscous liquid. In § 4, the resulting contact models are used in theoretical descriptions and simulations of the rheological properties of flowing suspensions of microscopically rough particles that experience particle–particle contacts, including several new results. Concluding remarks are presented in § 5.

2. Sphere moving down an inclined plane

The motion of a sphere down an inclined planar surface due to gravity provides a convenient method for analysing some of the basic features of solid–solid interactions in a viscous fluid. If a perfectly smooth sphere is in point contact with a perfectly smooth plane in a viscous fluid treated as a continuum, then the analysis of Goldman *et al.* (1967) predicts that the sphere will stick to the plane and not move under the action of a finite force, due to a weak singularity in the hydrodynamic resistance to tangential motion along the plane as the sphere–plane separation vanishes. However, experiments by Carty (1957) from a decade earlier showed that an apparently smooth sphere moves down an inclined plane with essentially constant velocity. Moreover, the observed translation and rotation of the sphere cannot be described by a purely hydrodynamic theory for any physical separation between the surfaces of the sphere and plane. The apparent paradox was resolved by Smart *et al.* (1993), who extended the hydrodynamic theory of Goldman *et al.* (1967) to include the effects of solid–solid contact friction, with a separation between the nominal surfaces of the sphere and the plane set equal to the measured value of the microscopic surface roughness.

According to the theory of Smart *et al.* (1993), the normal and tangential components of the force balance on the sphere in contact with the plane via microscopic asperities of uniform height δ are, respectively,

$$\tfrac{4}{3}\pi a^3 \Delta\rho g \cos\theta = F_{\mathrm{n}}, \tag{2.1}$$

$$\tfrac{4}{3}\pi a^3 \Delta\rho g \sin\theta = 6\pi\mu a(u\hat{F}_{\mathrm{t}} + a\omega\hat{F}_{\mathrm{r}}) + F_{\mathrm{f}}, \tag{2.2}$$

where a is the sphere radius, u is its translational speed, ω is its rotational speed, $\Delta\rho$ is the density difference between the sphere and fluid, g is the magnitude of the gravitational acceleration, θ is the angle of inclination of the plane from horizontal, μ is the fluid viscosity, and F_{n} and F_{f} are the normal and frictional (tangential) components of the solid–solid contact force, respectively. The hydrodynamic resistance coefficients are given by Goldman *et al.* (1967), based on the assumptions of creeping flow ($Re = \rho ua/\mu \ll 1$, where ρ is the fluid density) and that the microscopic surface roughness elements are sufficiently small and sparse to not change the hydrodynamic interactions from those for smooth surfaces at the same nominal separation:

$$\hat{F}_{\mathrm{t}} = -\tfrac{8}{15}\ln\xi + 0.9588, \tag{2.3}$$

$$\hat{F}_{\mathrm{r}} = \tfrac{2}{15}\ln\xi + 0.2526, \tag{2.4}$$

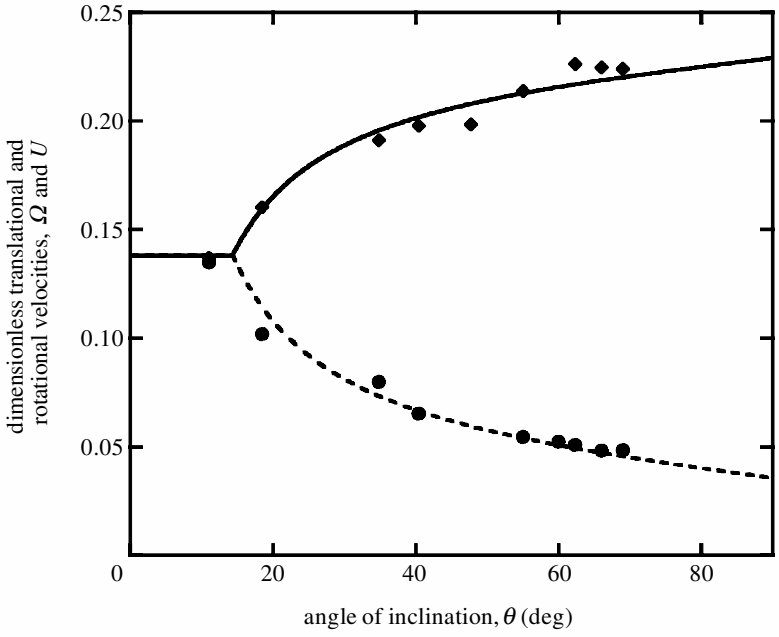

Figure 4. The dimensionless translational (diamonds) and rotational (circles) velocities of a Teflon sphere of diameter 0.635 cm and natural surface roughness of *ca.* 5 µm moving down an inclined plane in a viscous fluid. The translational (solid) and rotational (dashed) curves are calculated from the theory of Smart *et al.* (1993), with $\xi = 0.0015$ and $\mu_\mathrm{f} = 0.12$, while the experimental data (symbols) are previously unpublished results from our laboratory.

valid for $\xi = \delta/a \ll 1$. The torque balance about the centre of the sphere is

$$aF_\mathrm{f} = 8\pi\mu a^2(u\hat{T}_\mathrm{t} + a\omega\hat{T}_\mathrm{r}), \tag{2.5}$$

where

$$\hat{T}_\mathrm{t} = \tfrac{1}{10}\ln\xi + 0.1895, \tag{2.6}$$

$$\hat{T}_\mathrm{r} = -\tfrac{2}{5}\ln\xi + 0.3817. \tag{2.7}$$

For small angles of inclination, the sphere rolls without slipping, so that $u = a\omega$ from kinematic constraints. As the angle of inclination is increased, the normal component of the contact force is decreased while the frictional component is increased, until a critical angle is reached where $F_\mathrm{f} = \mu_\mathrm{f}F_\mathrm{n}$ (with μ_f the coefficient of rolling friction) and the sphere begins to slip as well as roll down the plane, with $u > a\omega$. The resulting expressions from solving (2.1)–(2.7) for the translational and rotational velocities, both with and without slip, are provided by Smart *et al.* (1993) and Galvin *et al.* (2001). The experiments of Smart *et al.* (1993) verify the predicted behaviour, but the particle motion showed variations or scatter in the measured velocities. Similar results have been obtained in our laboratory, such as those shown in figure 4. Following Smart *et al.* (1993), we define the dimensionless translational and rotational velocities as $U = u/(u_\mathrm{o}\sin\theta)$ and $\Omega = a\omega/(u_\mathrm{o}\sin\theta)$, respectively, where $u_\mathrm{o} = 2a^2\Delta\rho g/(9\mu)$ is the Stokes settling velocity of an isolated sphere.

King & Leighton (1997) observed that the effective hydrodynamic surface roughness or sphere–plane nominal separation is greater when the sphere is in motion than

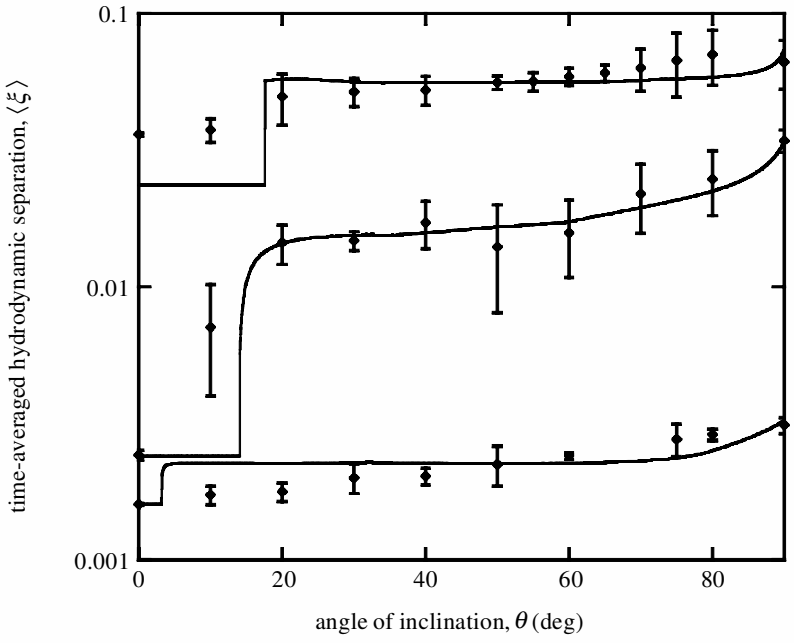

Figure 5. The average dimensionless hydrodynamic separation between a Teflon sphere of 0.635 cm diameter and a smooth acrylic plane as a function of the angle of inclination of the plane from horizontal. The theoretical curves and experimental data correspond to a naturally rough sphere with bump sizes from 5 to 10 µm, a sphere with a sparse coverage of 100 µm glass beads glued to its surface, and a sphere with a dense coverage of 100 µm glass beads glued to its surface (bottom to top). Adapted from Galvin *et al*. (2001).

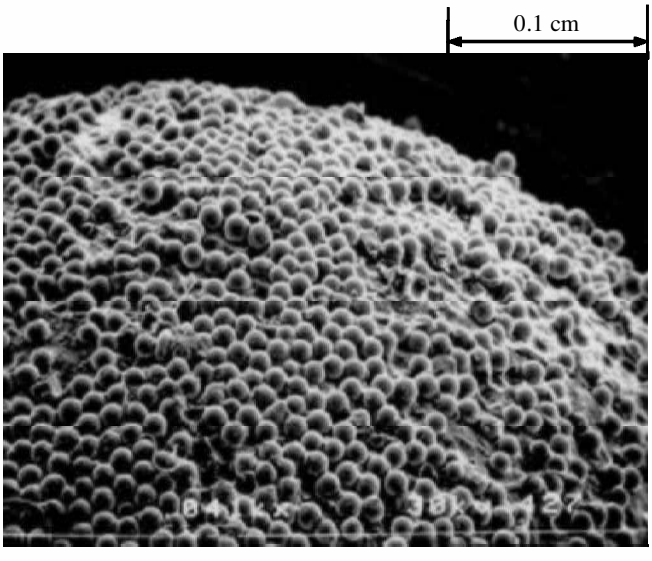

Figure 6. Scanning electron micrograph of a Teflon sphere of 0.635 cm diameter, densely covered with glass beads of 100 µm diameter glued to its surface.

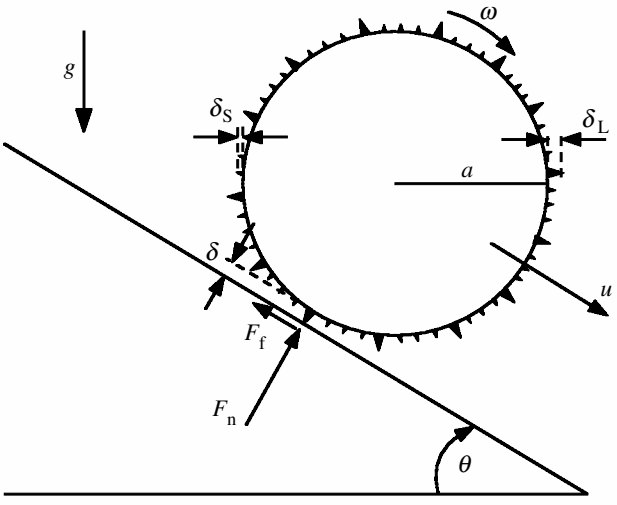

Figure 7. Schematic of a sphere with microscopic surface roughness (not to scale) composed of a sparse coverage of large bumps of height δ_{L} and a more dense coverage of small bumps of height δ_{S}. The nominal surface separation δ varies with time as the sphere moves down the inclined plane.

when it is at rest. Galvin *et al.* (2001) proposed that there are multiple roughness scales on the surface of the sphere which give rise to the data scatter and cause the average separation to increase when the sphere is in motion. They modelled the sphere surface as having a combination of small bumps with relatively large surface coverage and well-spaced larger bumps, and they modified the analysis of Smart *et al.* (1993) to account for the additional torque on the sphere when in contact with the plane via a large bump. The possibility of the loss of contact after an encounter with a large bump and before the sphere settles back to contact with the smaller bumps was also considered. Figure 5 shows their experimental data and model predictions for the time-averaged hydrodynamic separation of the nominal surfaces of the sphere and the plane versus the angle of inclination of the plane from horizontal. Nominal separations were measured using the method of Smart & Leighton (1989) by inverting the plane and timing the sphere as it fell away. The Teflon spheres had natural surface roughness with heights of 5–10 μm, while the typical roughness of the acrylic plane was less than 1 μm. A viscous oil with $\rho = 1.10$ g cm^{-3} and $\mu = 350$ g cm^{-1} s^{-1} was used. The lower curve in figure 5 is for an unmodified Teflon sphere with natural surface roughness, while the middle and upper curves are for modified Teflon spheres with 0.1 mm glass beads glued to their surfaces with low and high (see figure 6) surface coverages, respectively. There is good agreement between experiment and theory, using $\mu_{\mathrm{f}} = 0.15$ determined from the angle of repose under dry conditions.

The most striking result from figure 5 is that the average surface separation in all cases increases with increasing angle of inclination of the plane from horizontal. At small angles of inclination, the sphere is at rest, and the nominal surface separation is governed by the smaller roughness elements. As the angle of inclination is increased, the sphere rolls (and then rolls and slips beyond a critical angle) down the plane. When a large bump on the sphere makes contact with the plane, the sphere is lifted away from the plane to a greater nominal separation (see figure 7). After this

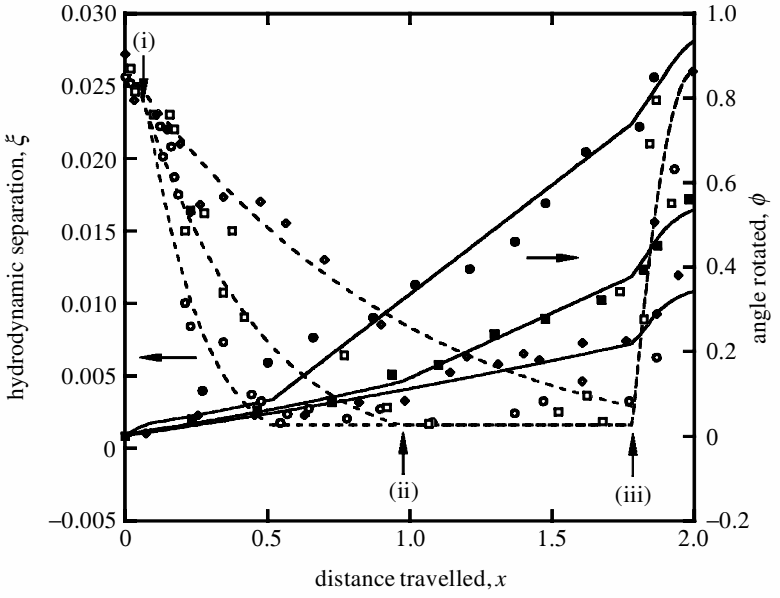

Figure 8. Dimensionless separation (dashed lines for theory and open symbols for experiments) and angle rotated (solid lines for theory and filled symbols for experiments) versus the dimensionless travel distance for a Teflon sphere of 0.635 cm diameter and 5 μm surface roughness moving down an acrylic plane with wires of 76 μm diameter stretched across it with spacing of 0.635 cm. The plane is inclined at $\theta = 30°$ (circles), 50° (squares) and 70° (diamonds) from horizontal. Arrows (i), (ii) and (iii) (shown for $\theta = 50°$) indicate when the sphere loses contact with the first wire, when the sphere then makes contact via its natural surface roughness, and when the sphere makes contact with the second wire, respectively. Adapted from Zhao *et al.* (2002), but with the model parameters changed to include the roughness of the sphere as it moved over a wire.

encounter, the sphere settles back toward the plane due to the normal component of gravity, while it continues to move down the plane due to the tangential component of gravity. The normal component of gravity becomes relatively weak as the plane becomes more vertical, and so the average separation increases with increasing angle of inclination and is governed by the height of the large bumps as $\theta \to 90°$. An increase in the nominal separation beyond that of the average roughness height for large angles of inclination was also observed by Prokunin (1998). For the dense coverage of glass beads (top curve in figure 5), the dimensionless separation of $\langle\xi\rangle = 0.07$ at $\theta \approx 90°$ corresponds to $\delta = 200\,\mu\text{m}$, representing large bumps composed of two glass beads (as apparent in figure 6). For the sparse coverage of glass beads (middle curve in figure 5), the dimensionless separation of $\langle\xi\rangle = 0.035$ at $\theta \approx 90°$ corresponds to $\delta = 100\,\mu\text{m}$, representing large bumps composed of well-spaced, single glass beads.

Zhao *et al.* (2002) extended the study of Galvin *et al.* (2001) to an artificially roughened plane, with a well-defined geometry formed by stretching small wires of known diameter across the plane at set distances down the plane. This geometry allows for pointwise measurements of the sphere's translational and rotational velocities and of its separation from the nominal surface of the plane. Figure 8 shows typical results for the hydrodynamic separation versus the distance (made dimen-

sionless by the sphere radius) that the sphere has travelled down the channel starting from the apex of one of the wires. The nominal separation was determined by inverting the plane and timing the sphere as it fell away from the plane using the method of Smart & Leighton (1989). The three different curves are for $\theta = 30°$, $50°$ and $70°$ (left to right). After travelling a short distance, the sphere loses contact with the wire. The dimensionless separation ξ decreases gradually while there is no solid–solid contact, with the motion normal to the plane resisted solely by lubrication, and is then nearly constant during the period of contact with the small bumps. Finally, contact with a second wire occurs, and there is a rapid increase in the dimensionless separation as the sphere rises over the wire. With increasing angle of inclination of the plane from horizontal, the motion of the sphere toward the plane during the period without contact becomes slower, due to the smaller normal component of gravity, and contact with the small bumps on the plane is not made for the largest angle investigated ($\theta = 70°$) before a second large bump (wire) is encountered. Figure 8 also shows the angle that the sphere rotated since the apex of the first wire. The rate of rotation of the sphere relative to its translation rate increases when the small bumps are encountered and then again when the second large bump is reached, due to friction. Also, the relative amount of rotation of the sphere is greater at smaller angles of inclination of the plane, because the large component of the gravity vector normal to the plane gives rise to higher friction during contact with the small bumps and, hence, less slip and more rotation.

3. Heavy sphere settling past a light sphere

We have further examined the nature of solid–solid contacts in a viscous fluid by considering the gravitational sedimentation of a heavy sphere past a light sphere (Zhao & Davis 2002). As noted previously, if the spheres are perfectly smooth and the fluid is considered to be a continuum, then lubrication forces prevent physical contact from occurring. In this case, due to the linearity and reversibility of the creeping flow equations, the trajectory of each sphere will have fore-and-aft symmetry about a horizontal plane at the location where the line of centres of the two spheres becomes vertical. However, Zeng *et al.* (1996) showed that spheres with microscopic surface roughness may experience solid–solid contact when the separation between their nominal surfaces becomes comparable with the heights of the roughness elements. Since the contact forces are irreversible (compressive when $\theta < 90°$, but not tensile when $\theta > 90°$), the symmetry of the sphere trajectories is broken, as illustrated in figure 9.

Experimental data showing asymmetric relative trajectories for a heavy Teflon sphere ($\rho_1 = 2.15\ \mathrm{g\,cm^{-3}}$, $a_1 = 0.318$ cm) falling past a light nylon sphere ($\rho_2 = 1.13\ \mathrm{g\,cm^{-3}}$, $a_2 = 0.318$ cm) in a viscous fluid ($\rho = 1.11\ \mathrm{g\,cm^{-3}}$, $\mu = 403\ \mathrm{g\,cm^{-1}\,s^{-1}}$ at 22 °C) are shown in figure 10. The thin lines were calculated from the theory of Zhao & Davis (2002) and are for a Teflon sphere artificially roughened by gluing small glass beads of diameter 0.1 mm to its surface. Even though the two corresponding experiments had different initial horizontal offsets ($\Delta\hat{y}_0 = 0.28$ and 0.48, when made dimensionless by the particle radius), they have the same final dimensionless horizontal offset ($\Delta\hat{y}_\mathrm{f} = 0.83$), which exceeds the initial offsets and indicates that irreversible contacts occurred. Moreover, the initial condition for the downstream portion of the trajectory that yields this final offset is $\xi = 0.036$ at $\theta = 90°$, which

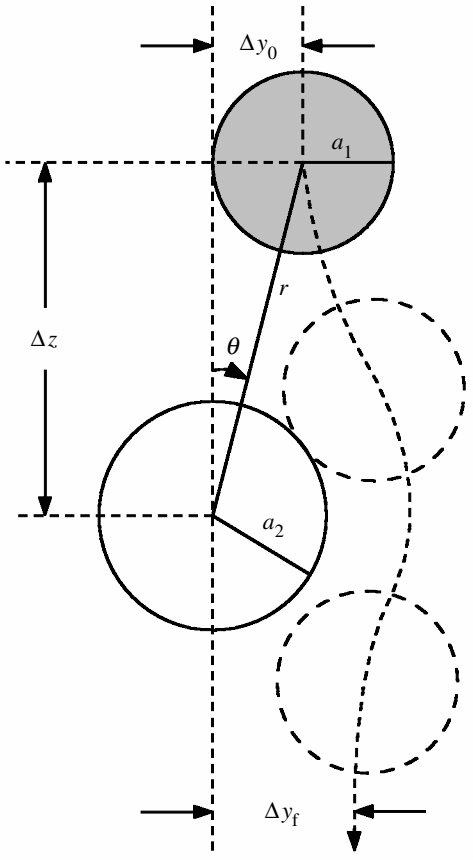

Figure 9. Gravitational motion of a heavy sphere (shaded initial location) relative to a neighbouring light sphere. Contact occurs for a portion of the upper part of the relative trajectory ($\theta < 90°$) but is then lost for the lower part of the trajectory ($\theta > 90°$) because the contact is not able to impart a tensile force. As a result, the trajectory symmetry is broken and the final horizontal offset exceeds the initial horizontal offset.

corresponds to a dimensionless separation of $\delta = 110\,\mu\text{m}$ and is essentially equal to the roughness height created by the small glass beads attached to the heavy sphere's surface. The thick line in figure 10 ($\Delta\hat{y}_0 = 0.43$, $\Delta\hat{y}_f = 0.68$) was also calculated from the theory of Zhao & Davis (2002) and is for a naturally rough Teflon sphere. The initial separation for the downstream part of the relative trajectory is much smaller in this case ($\xi = 0.0026$ at $\theta = 90°$) and corresponds to a dimensional roughness height of $\delta = 8\,\mu\text{m}$, which is consistent with scanning electron micrographs of the sphere surfaces and with hydrodynamic measurements of the natural surface roughness using the method of Smart & Leighton (1989). Additional experiments with different initial horizontal offsets for the unmodified Teflon sphere show essentially the same final offset (Zeng *et al.* 1996; Zhao & Davis 2002). The smaller separation at $\theta = 90°$ for the naturally rough Teflon sphere gives rise to a smaller final horizontal offset compared with that for the artificially roughened sphere.

The asymmetry of the trajectories in figure 10 is indicative of particle–particle contacts, but it does not provide information to characterize the nature of the resulting contact forces or whether the two spheres move in rigid-body rotation while in contact

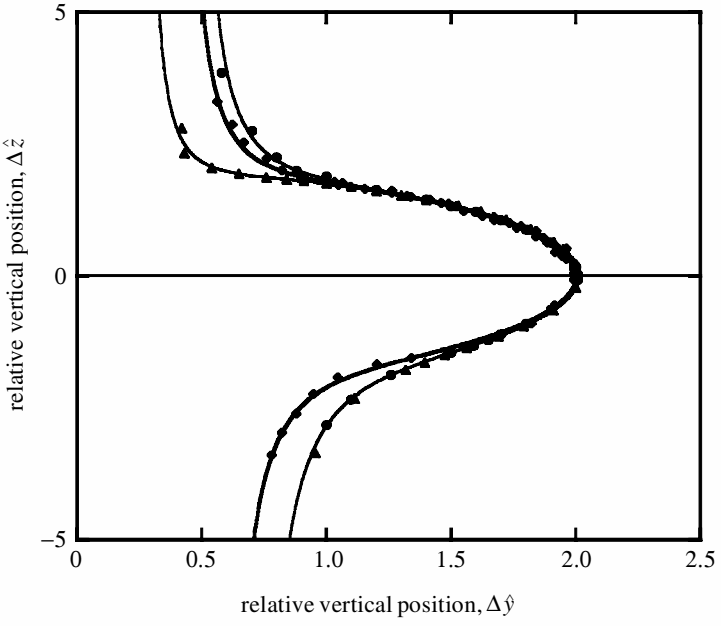

Figure 10. Relative trajectories of a heavy Teflon sphere falling past a light nylon sphere of the same size (0.635 cm diameter) in a viscous fluid. The thin lines (theory), triangles (experiments with $\Delta\hat{y}_0 = 0.28$) and circles (experiments with $\Delta\hat{y}_0 = 0.48$) are for a Teflon sphere with its surface modified by the attachment of glass beads of 0.1 mm diameter, while the thick line (theory) and diamonds (experiments with $\Delta\hat{y}_0 = 0.43$) are for an unmodified Teflon sphere with surface asperities of less than 10 μm in height. The results for the unmodified Teflon sphere are from Zhao & Davis (2002).

or if the heavy sphere rolled and/or slipped around the surface of the light sphere. To address these issues, Zhao & Davis (2002) performed microvideo experiments with ink dots placed on the sphere surfaces. The image frames were then analysed to determine the rotational (as well as translational) motion of each of the two interacting spheres in gravity sedimentation. Figure 11 shows the angle that each sphere rotated versus the angle between the line of centres and vertical. The heavy sphere is 0.635 cm in diameter and made of Teflon. The light sphere is 0.635 cm in diameter and made of nylon, with 0.1 mm glass beads glued on the surface of the nylon sphere with a sparse distribution. Contact first occurred at $\theta \approx 15°$, and rolling-without-slipping theory is used to add the angle each sphere would have rotated if in contact for $0° < \theta < 15°$. The 45° line (dotted) represents the stick/rotate model described by Davis (1992) in which rigid-body rotation occurs,

$$\omega = \omega_1 = \omega_2, \tag{3.1}$$

where $\omega = \mathrm{d}\theta/\mathrm{d}t$ is the rate of rotation of the line of centres, and ω_1 and ω_2 are the rotational speeds of the heavy and light spheres, respectively. Clearly, rigid-body rotation is not observed, as the light sphere rotates faster than the line of centres while the heavy sphere rotates more slowly than the line of centres. This finding is because the shear stress on the outer edge (away from the contact point) of the heavy sphere slows its rotation, while that on the outer edge of the light sphere aids its rotation. Note that positive rotation is in the clockwise direction (see figure 9).

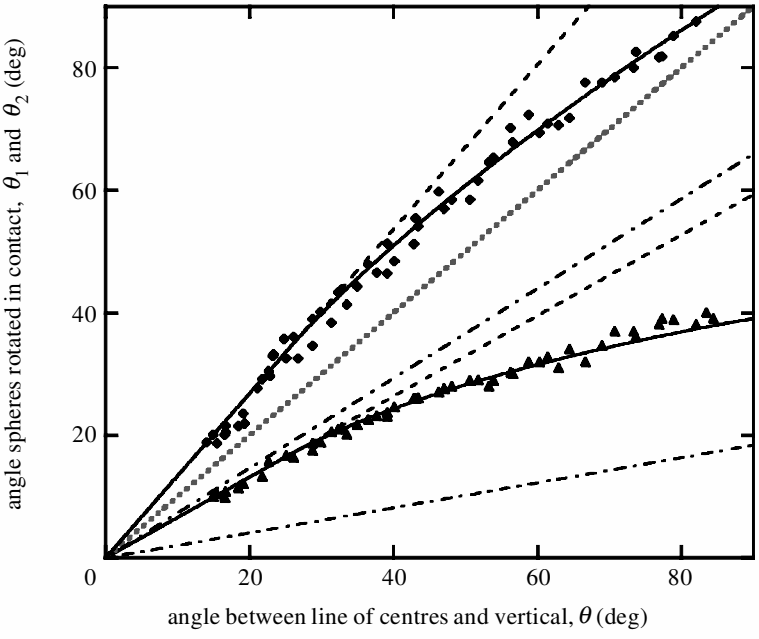

Figure 11. Angles which the heavy (triangles) and light (diamonds) spheres rotated versus the angle between the line of centres and vertical for a Teflon sphere falling past an artificially roughened nylon sphere of the same size (0.635 cm diameter). The dotted 45° line is the stick/rotate model, the dashed lines are for rolling without slipping, the dot–dashed lines are for free slipping, and the solid curves are the roll–slip model of Davis (1992) with a fitted friction coefficient of $\mu_f = 0.2$; the upper and lower sets of curves are for the light and heavy spheres, respectively. The data are from Zhao & Davis (2002).

It is also apparent from figure 11 that a simple hard-sphere model, where the spheres are prevented from approaching each other more closely than a dimensionless separation ξ, but then freely slip around each other with no solid–solid friction, does not describe the observed behaviour. Instead, the spheres roll around each other without slipping, until the slipping angle of $\theta_s \approx 25°$, which corresponds to a friction coefficient of $\mu_f \approx 0.2$, is reached. After that, the spheres rotate more slowly due to slipping, and their rotational velocities are well described by the roll–slip model of Davis (1992) with $\mu_f \approx 0.2$.

The issue of slipping is examined more closely in figure 12. If the two spheres rotate without slipping when in contact, then kinematic constraints require that

$$(a_1 + a_2)\omega = a_1\omega_1 + a_2\omega_2. \tag{3.2}$$

From noting that $\omega = \mathrm{d}\theta/\mathrm{d}t$, $\omega_1 = \mathrm{d}\theta_1/\mathrm{d}t$ and $\omega_2 = \mathrm{d}\theta_2/\mathrm{d}t$, and then integrating this equation, we define a slip ratio as $(\theta_1 + \theta_2)/(2\theta)$. This ratio is unity for rolling without slipping. The data in figure 12 show (with some scatter) that rolling without slipping occurred for $\theta < 25°$, and that slipping occurred for larger angles due to the smaller component of gravity pushing the spheres together along their line of centres. Again, the data are well fitted by the roll–slip model with $\mu_f \approx 0.2$.

The scatter of the data in figures 10–12 is thought to be due to the statistical nature of the microscopic roughness on the sphere surfaces, where the asperities are

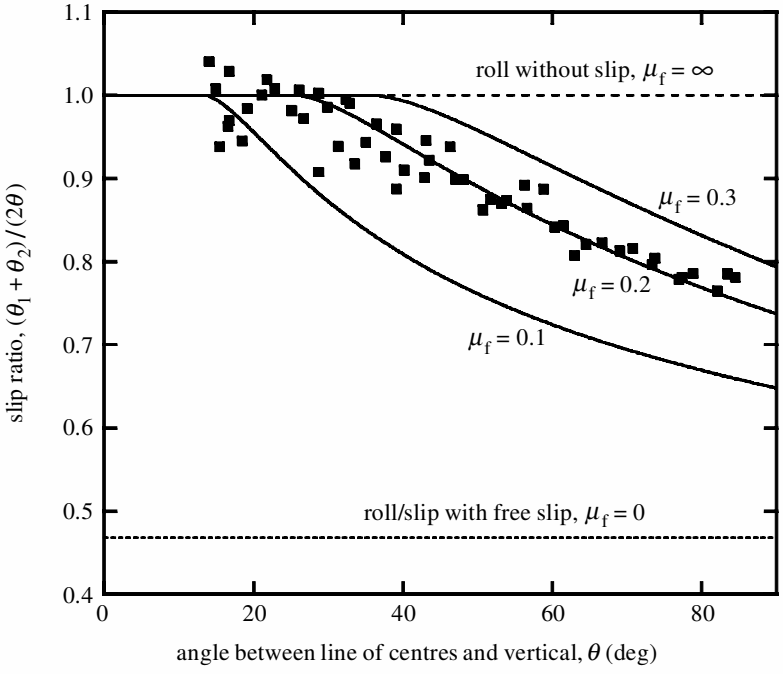

Figure 12. Slip ratio versus the angle between the line of centres and vertical for a Teflon sphere falling past an artificially roughened nylon sphere of the same size (0.635 cm diameter). The solid lines are the roll–slip model of Davis (1992), with a friction coefficient of $\mu_f = 0.2$ providing the best fit. Adapted from Zhao & Davis (2002).

not of uniform size or spacing. Besides causing the rotational motion to be non-uniform, the nominal separation between the sphere surfaces will vary as bumps of different sizes are encountered. We recently developed a method to determine the nominal separation by rotating the tank about a horizontal axis until the heavy sphere was directly below the light sphere, and then measuring the time it took the heavy sphere to fall from its initial separation below the light sphere to each of two specified small separations; the initial separation was then determined using two-sphere mobility functions (Zhao & Davis 2003). Figure 13 shows results for a Teflon heavy sphere and a nylon light sphere, both of 0.635 cm diameter, where two roughness sizes were created by placing small glass beads (0.1 mm diameter) at well-spaced intervals around the surface of the naturally rough Teflon sphere. After the spheres made contact in the viscous fluid described previously (Zhao & Davis 2002), they were allowed to interact until $\theta \approx 22°$, 49° or 86°, at which point the tank was rotated and the nominal separation was determined from the fall rate of the heavy sphere from below the light sphere. As expected, the data show a broad distribution of separations of the nominal surfaces, spanning the range of the natural roughness heights ($\delta \approx 10\,\mu\text{m}$, $\xi \approx 0.0035$) to the diameter of the glass beads glued to the surface of the Teflon sphere ($\delta = 100\,\mu\text{m}$, $\xi = 0.035$). Moreover, there is a general trend of increasing average separation with increasing angle of inclination of the line of centres from the vertical. As $\theta \to 90°$, the data become clustered at $\xi \approx 0.035$, indicating that the size of the largest bumps dominates at the point where the two spheres separate. This result, as also seen in figure 10, is because the component of

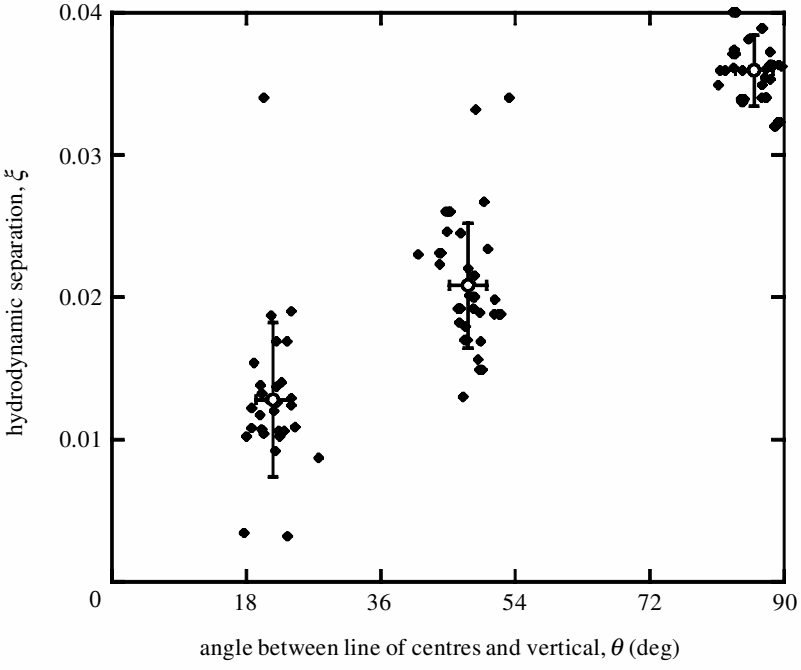

Figure 13. Hydrodynamic separation between the nominal surfaces of an artificially roughened Teflon sphere falling past a nylon sphere of the same size in a viscous fluid, starting from many different initial conditions. The error bars represent plus and minus one standard deviation for data clustered around three selected angles between the line of centres and vertical. Data taken from Zhao & Davis (2003).

gravity normal to the sphere surfaces near contact becomes weak as $\theta \to 90^\circ$ and is unable to drive the spheres back together after a large bump lifts them apart. We have recently developed a theory to describe the interaction of two spheres with multiple roughness heights (Zhao & Davis 2003).

4. Particle contact effects on suspension rheology

In this section, we introduce the wider effects of interparticle contacts. In particular, we are interested in the influence that they can have on the macroscopic flow of a suspension of rough particles. Based on the experimental verification of the previous section, we consider the frictional roll–slip contact model of Davis (1992) and compare it with those results which are available for smooth spheres.

(*a*) *Dilute suspensions in three dimensions*

The rheology of a dilute suspension of non-Brownian spheres at small Reynolds number was first studied by Einstein (1906), who calculated the viscosity to $O(c)$ of a suspension containing smooth spheres at volume concentration c. Batchelor & Green (1972*a*) extended this work to $O(c^2)$, for which they had to consider the interactions between pairs of particles (whereas Einstein had looked at particles in isolation). To calculate the stress, they used an integral of the extra stress contributed by a pair of particles in a given configuration, multiplied by the probability of finding a

pair of particles in that configuration: the *pair-distribution function*. There were two difficulties with this work. The first, an integral which was not uniformly convergent, they solved by extracting a term of $\frac{5}{2}c^2$ to renormalize the integral. The second was in the pair-distribution function. They showed that, for any trajectory of one particle relative to the position of another, the pair distribution on that trajectory could be expressed as $p(\boldsymbol{r}) = Cq(s)$, with $\boldsymbol{r}$ the vector from the centre of particle 1 to the centre of particle 2, and s the dimensionless particle separation. The constant C can be determined from boundary conditions for any bound trajectories for which s remains finite for all time. In a shear flow, there is an infinite region of space occupied by these closed orbits, on which the pair distribution (and hence the stress contribution) cannot be uniquely determined. The distance of closest approach away from the plane of shear on these trajectories is arbitrarily large, so roughness will not destroy them and the shear viscosity cannot be calculated, even for rough particles. Smart & Leighton (1989) calculated the pair distribution in the plane of shear and showed experimental results of the same form; our analysis agrees with theirs in the relevant parts of the flow. More recently, Brady & Vicic (1995) investigated the same situation with Brownian motion present, in which case the distribution function can be everywhere determined numerically, even in the absence of roughness.

For any flow without bound trajectories, Batchelor & Green (1972*a*) showed that the effective viscosity for smooth spheres in a fluid of viscosity μ is given by

$$\eta = \mu(1 + \tfrac{5}{2}c + kc^2 + O(c^3)), \tag{4.1}$$

where, for smooth spheres,

$$k = \frac{5}{2} + \frac{15}{2}\int_2^\infty J(s)q(s)s^2\,\mathrm{d}s, \tag{4.2}$$

$$q(s) = (1 - A(s))^{-1}\phi^{-3}(s), \tag{4.3}$$

$$J(s) = K(s) + \tfrac{2}{3}L(s) + \tfrac{2}{15}M(s), \tag{4.4}$$

$$\phi(s) = \exp\left[\int_s^\infty \frac{(A(s') - B(s'))\,\mathrm{d}s'}{(1 - A(s'))s'}\right], \tag{4.5}$$

and the mobility functions (A, B, K, L, M) are those from Batchelor & Green (1972*b*). The $O(c)$ term was calculated by Einstein (1906).

We begin by considering axisymmetric strain flows, for which there are no closed orbits and (4.1) holds for smooth spheres. When roughness is introduced, we have to consider several regions of the flow: regions of the trajectories not involved in contact and where roughness makes no difference; regions of particle–particle contact; dense regions where particles move away from one another after contact; and empty regions which particles cannot access because to do so would involve passing through closer nominal separations than the roughness permits.

The interparticle velocities of two particles in contact are derived from lubrication theory and given on p. 430 of Wilson & Davis (2002)—a small correction of the forms given in Wilson & Davis (2000). The other regions have velocities as derived by Batchelor & Green (1972*b*). A symmetry argument shows that the stress must be Newtonian in the sense that it can be represented by a scalar viscosity, and corrected plots of the c^2 term of this viscosity are shown in figures 14 and 15 for biaxial and uniaxial expansion, respectively. This viscosity coefficient in (4.1) is $k \approx 6.9$

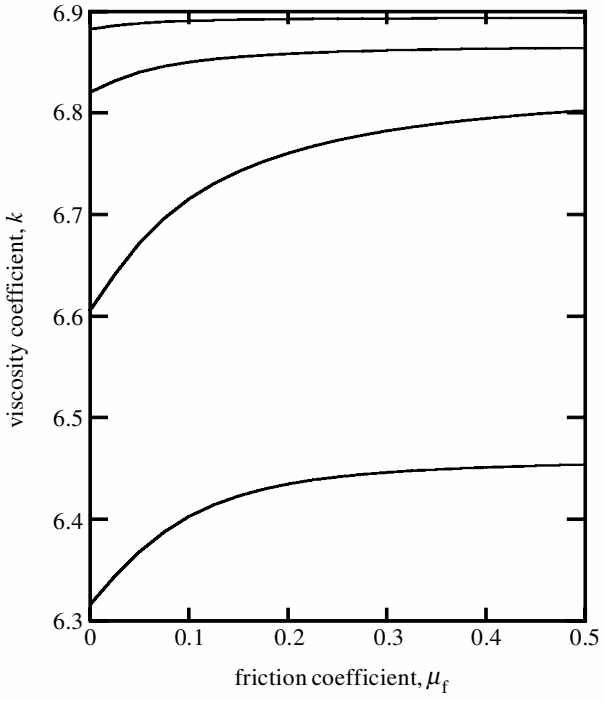

Figure 14. Plot of the c^2 coefficient of viscosity against the friction coefficient for biaxial expansion flow of a dilute suspension of solid particles. Effective roughness heights are $\xi = 10^{-7}$, 10^{-5}, 10^{-3} and 10^{-2} (top to bottom). Corrected from Wilson & Davis (2000).

for smooth spheres, in both uniaxial and biaxial expansion. The viscosity decreases strongly with increasing roughness height, and it increases weakly with increasing friction coefficient. The former seems counterintuitive, but in fact the major effect of the roughness is to remove particles from the small-gap region in which lubrication stresses contribute strongly to the overall dissipation.

For shear flows, although we cannot calculate the viscosity, without assuming values for the pair-distribution function in the region of closed orbits, a symmetry argument allows us to calculate the dimensionless first and second normal stress differences, N_1 and N_2, as defined in Wilson & Davis (2000). The results for no tangential friction, $\mu_f = 0$, are plotted against roughness height in figure 16. It can be seen that the normal stresses are both negative and increase in magnitude with increasing roughness height. For values of ξ below 2.1×10^{-4}, no unbounded trajectories are affected by the roughness, so both normal stress differences are zero. There is very little dependence on the friction coefficient, μ_f.

(*b*) *Shear of dilute suspensions in two dimensions*

In this section, we consider shear flow of a monolayer of spheres whose centres all lie on one plane (the plane of shear) in an infinite fluid and which do not leave that plane under the action of the shear flow. We define the area concentration of spheres, c, to be the proportion of the area of the plane of centres which is occupied by solids; thus, the volume fraction of the slice of width $2a$ containing all the spheres is $\frac{2}{3}c$.

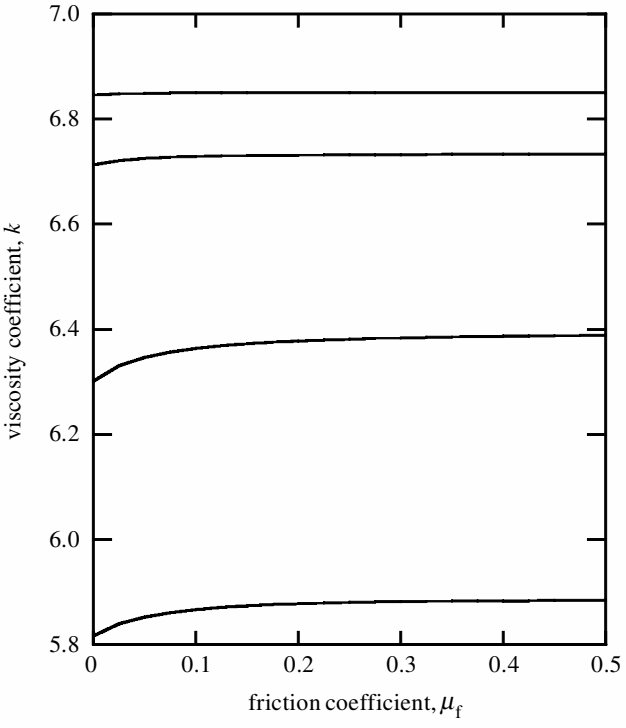

Figure 15. Plot of the c^2 coefficient of viscosity against the friction coefficient for uniaxial expansion flow of a dilute suspension of solid particles. Effective roughness heights are $\xi = 10^{-7}$, 10^{-5}, 10^{-3} and 10^{-2} (top to bottom). Corrected from Wilson & Davis (2000).

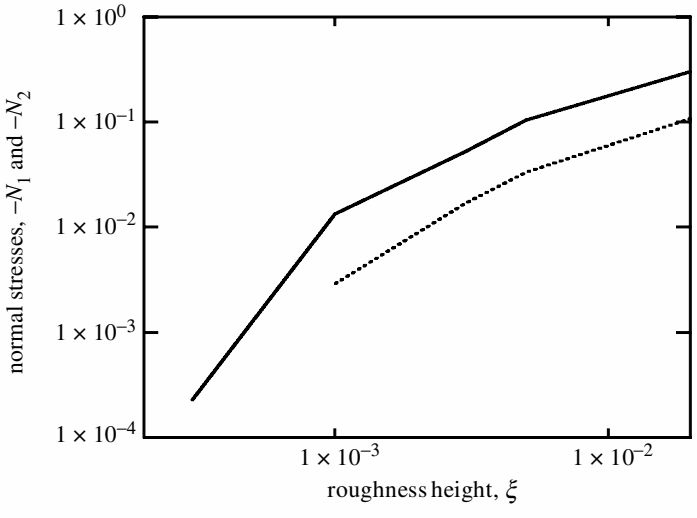

Figure 16. The negative normal stress differences (scaled with $c^2\mu|\dot{\gamma}|$, where $\dot{\gamma}$ is the shear rate) plotted against the dimensionless effective roughness height for shear flow of a dilute suspension of solid particles with no tangential friction, $\mu_f = 0$, with the solid curve representing $-N_1$ and the dashed curve representing $-N_2$. Corrected from Wilson & Davis (2000).

The symmetry of the system guarantees that the second normal stress difference, N_2, is related to the first by $N_2 = -\frac{1}{2}N_1$, as has been seen experimentally in three-dimensional flow by Laun (1994). We consider the behaviour of the effective viscosity, η, and the first normal stress difference, N_1.

For smooth spheres, the problem of closed orbits (discussed in § 4 *a*) persists, and we cannot calculate an unambiguous viscosity. For a planar straining flow or other steady planar flow without closed orbits, the viscosity follows the pattern of (4.1), with modifications because of the two-dimensional geometry:

$$\eta = \mu\left(1 + \tfrac{5}{3}c + c^2\left\{\frac{20}{3}\int_2^\infty \tilde{J}(s)\tilde{q}(s)s\,\mathrm{d}s\right\}\right), \tag{4.6}$$

where

$$\tilde{q}(s) = (1 - A(s))^{-1}\phi^{-2}(s) \quad \text{and} \quad \tilde{J}(s) = K(s) + L(s) + \tfrac{1}{4}M(s). \tag{4.7}$$

The mobility functions are the standard expressions from Batchelor & Green (1972*b*), and $\phi(s)$ is as defined in (4.5) above; note that the different form given in eqn (2.8) of Wilson & Davis (2002) is a typographical error. We can see that the equivalent of the Einstein (1906) viscosity result at $O(c)$ has a coefficient of $\frac{5}{3}$, as opposed to $\frac{5}{2}$ in three dimensions; this difference is simply a result of the new definition of particle fraction.

Once roughness is introduced, because every closed orbit has a distance of closest approach of less than $2.1 \times 10^{-4}a$, any realistic value of the effective roughness height ξ allows us to break all closed orbits, thus permitting full calculation of the pair-distribution function and hence the steady-state stress. The results for shear viscosity, η, and first normal stress difference, N_1, are plotted in the next subsection with the results for concentrated monolayers. In summary, the results are very similar to those for three-dimensional flows (viscosity from straining flows, normal stress from shear). The first normal stress difference N_1 is zero if $\xi < 2.1 \times 10^{-4}$ and otherwise an $O(c^2)$ quantity, negative, and larger in magnitude for larger values of ξ. The viscosity decreases with increasing roughness height, and both terms of the rheology are almost independent of the friction coefficient, μ_f.

(*c*) *Concentrated monolayers*

For concentrated suspensions, direct analytical methods are no longer applicable, so instead we use numerical simulation to investigate the effects of the contact forces. We consider shear flow of a viscous fluid containing identical spheres of radius a, as before, but because of the computational time involved, we restrict consideration to a monolayer of spheres, as in § 4 *b*. The Stokesian dynamics (SD) method, invented by Durlofsky *et al.* (1987), computes the hydrodynamic interactions among a large number of suspended particles using a self-consistent combination of two-body interactions. The details of the SD method are covered in depth in, for example, Brady & Bossis (1988).

For our calculation, we need to determine the contact forces acting at each contact point between two particles. We begin by assuming all particles to be force free and torque free and then calculate their translational and rotational velocities under the imposed bulk fluid flow. We then identify each pair of particles that will be in compressive contact and use their velocities to calculate the lubrication approximation

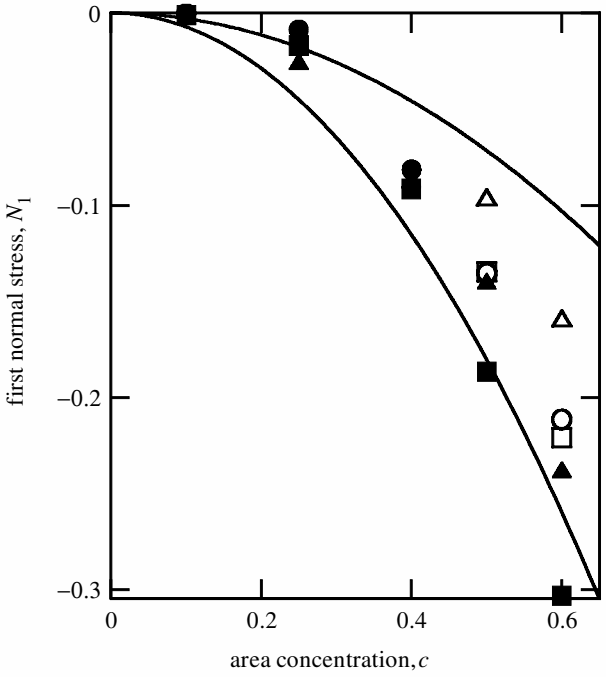

Figure 17. The first normal stress difference (scaled with $\mu|\dot{\gamma}|$) versus area fraction for shear flow of a monolayer of solid spheres with roughness heights of $\xi = 10^{-2}$ (triangles), 10^{-3} (squares) and 10^{-4} (circles) and no tangential friction ($\mu_f = 0$). The closed symbols are for the full SD code, and the open symbols are for the MSD code. The curves represent the theoretical prediction for dilute suspensions, with the lower curve for $\xi = 10^{-2}$ and the upper for $\xi = 10^{-3}$; the dilute prediction for $\xi = 10^{-4}$ is $N_1 = 0$, because no unbounded trajectory is broken at this roughness height and so each trajectory has fore-and-aft symmetry. The full SD results for $\xi = 10^{-2}$ and 10^{-3} are from Wilson & Davis (2002).

to the contact force between the particles. This calculation, which uses the near-field forms of the two-sphere mobility functions given in Kim & Karrila (1991), is given in eqns (3.1) and (3.2) of Wilson & Davis (2002). Of course, for concentrated systems it is possible (and indeed likely) that a single particle will be in contact with more than one other particle at once. In this case, the contact forces and torques occurring from each contact are simply added to give the total contact force and torque acting on the particle in question. It should be noted that, despite the multiple contacts, this system is still dominated by hydrodynamic (viscous) forces, and is quite different from a slow granular flow (e.g. Savage 1998) in which the contact forces are the only ones present.

In addition, for very concentrated suspensions (area fraction $c > 0.5$), we have developed a modified SD program (MSD) which only includes near-field, lubrication and contact interactions. These contributions to the stress and to the flow will dominate over far-field contributions when the particles are closely packed. By efficient storage and manipulation of the sparse matrices involved, this new algorithm is $O(N)$ in the number of particles per periodic cell, so we can consider many more particles with only a minor loss of accuracy.

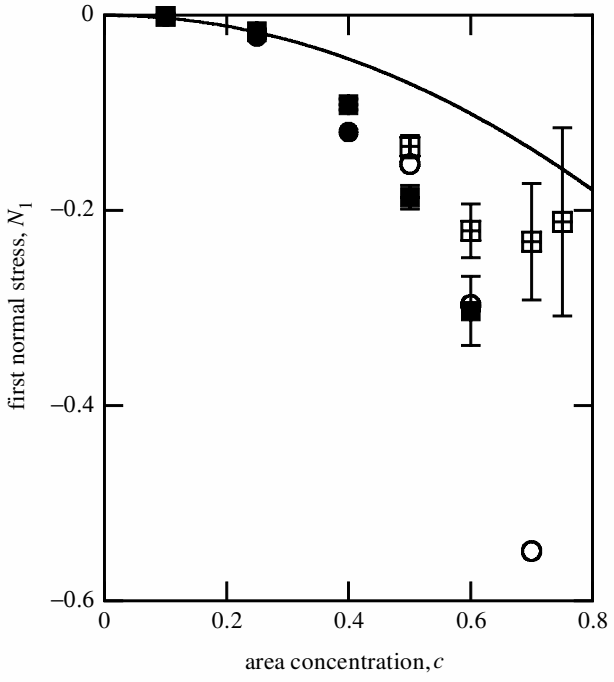

Figure 18. The first normal stress difference (scaled with $\mu|\dot{\gamma}|$) versus area fraction for shear flow of a monolayer of solid spheres with a roughness height of $\xi = 10^{-3}$ and tangential friction of $\mu_f = 0$ (squares) and 0.5 (circles). The closed symbols are from the SD code, and the open symbols are from the MSD code. The curve represents the dilute theory for both cases, as the results are indistinguishable on this scale. Error bars representing plus and minus one standard deviation for eight simulations are shown (for clarity) only for the cases in which $\mu_f = 0$.

5. Results and discussion

Some results for concentrations up to $c = 0.6$ are given in Wilson & Davis (2002). These results came from the full SD code, using 25 particles per periodic cell and integrating forward in time for 200 shear units (i.e. $\dot{\gamma}t = 200$, where $\dot{\gamma}$ is the shear rate and t is time). Here, we present additional results from this program, along with the first results from the MSD program. In the latter, we use 200 particles per periodic cell and integrate for 50 shear units. In all cases, we discard the first 10 shear units of the run, in which period the initial configuration of the particles remains important, and average over later time periods when a stochastic steady state has been reached. Note that the contact forces make this system irreversible, so that the particles do not return to their initial positions if the shear direction is reversed. Even for smooth spheres, the apparently deterministic system (with Brownian motion neglected) proves to be chaotic due to many-particle interactions and will not return to its initial configuration after flow reversal if the initial strain is large.

Figures 17 and 18 consider the first normal stress difference, N_1. Here, we find that N_1 is negative for all parameter values, but the trends are much less clear. For moderate concentrations ($c = 0.5$, 0.6) we have two sets of results: one from the full SD simulation with 25 particles, and the other from the MSD simulation with 200 particles. In all cases, the MSD result gives a lower value for the magnitude of N_1.

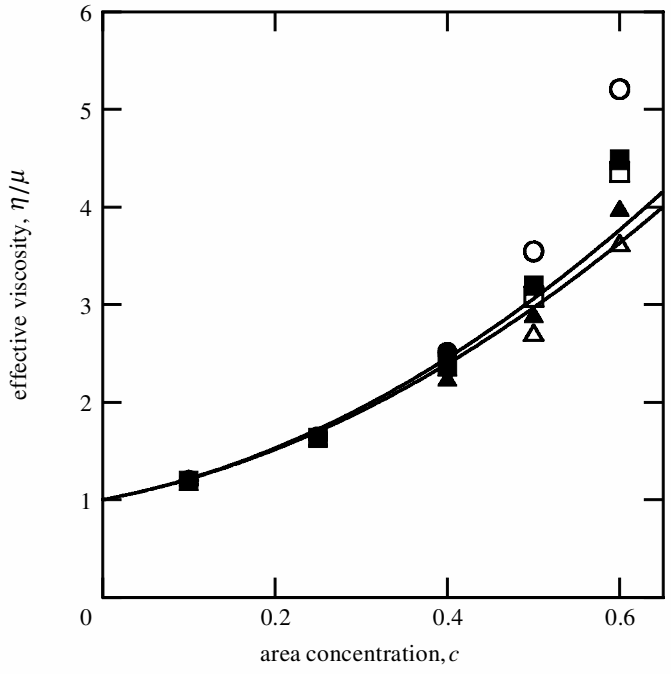

Figure 19. Dimensionless effective viscosity versus area fraction for shear flow of a monolayer of solid spheres with roughness heights of $\xi = 10^{-2}$ (triangles), 10^{-3} (squares) and 10^{-4} (circles) and no friction. The closed symbols are from the full SD code, and the open symbols are from the MSD code, which neglects dissipation due to far-field interactions. The curves represent the theoretical prediction for dilute suspensions, with the lower curve being for $\xi = 10^{-2}$ and the upper for $\xi = 10^{-3}$. There is no dilute prediction for $\xi = 10^{-4}$, because not all of the bounded trajectories are broken at this roughness height and the pair-distribution function is indeterminate.

Unfortunately, the discrepancies between the two calculation methods are greater than the differences between the results for the different roughness heights or the different friction values. Even the trend against concentration is not entirely clear; in general, the magnitude of N_1 increases with increasing concentration, but there is a decrease in the magnitude of N_1 predicted by the MSD code between $c = 0.7$ and $c = 0.75$ for $\xi = 10^{-3}$ and $\mu_f = 0$. The reliability of the MSD approach, which neglects far-field interactions, for normal stress calculations must be put in doubt by these results. There are large fluctuations in these values with time during the simulation (this phenomenon has also been observed by Phung *et al.* (1996) and Morris & Katyal (2002)), as well as large differences between repeated simulations with different initial configurations (as the error bars in figure 18 demonstrate). Thus, the non-monotonic behaviour may simply be a fluctuational effect.

In figures 19 and 20, we look at the dependence of the shear viscosity on the two parameters of the contact model. Here, the results from the two different calculation methods are entirely consistent, with MSD slightly underestimating viscosities as it must do by neglecting far-field dissipation. From figure 19, it is clear that increasing the roughness height decreases the viscosity, even for quite large concentrations. In figure 20, we see that the tangential friction, which makes little difference for dilute

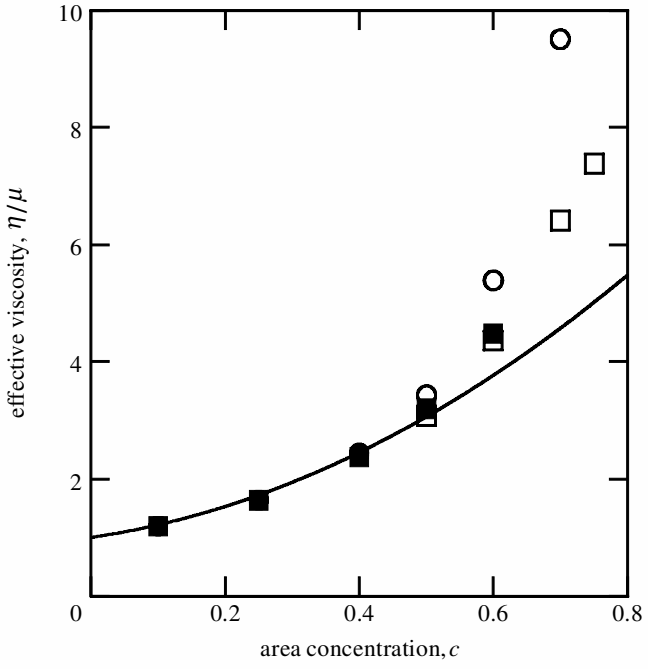

Figure 20. Dimensionless effective viscosity is plotted against area fraction for shear flow of a monolayer of solid spheres with a roughness height of $\xi = 10^{-3}$ and tangential friction of $\mu_f = 0$ (squares) and 0.5 (circles). The closed symbols are for the full SD scale, and the open symbols are for the MSD code, which neglects dissipation due to far-field interactions. The smooth curve represents the dilute theory, for which the results for the two friction coefficients are indistinguishable on this scale.

suspensions in that the $O(c^2)$ curves for $\mu_f = 0$ are indistinguishable, causes a large increase in viscosity at high concentrations (an increase of almost 50% at $c = 0.7$, $\xi = 10^{-3}$).

6. Concluding remarks

Experiments with a heavy sphere moving down an inclined plane or past a lighter sphere due to gravity in a viscous fluid show that solid–solid contacts occur due to microscopic surface roughness. These contacts cause the sphere(s) to undergo a combination of rolling and slipping, and they break the fore-and-aft symmetry of the trajectories predicted for two smooth spheres interacting in a viscous fluid at low Reynolds number. Analysis of the translational and rotational motions shows that they are well described by modified hydrodynamic descriptions that include solid–contact friction. Moreover, the motion of the heavy sphere down the plane or past the light sphere is not smooth during contact, and measurements of the nominal surface separation show variations in its value between the heights of small and large surface asperities. As the angle of the line of centres, or of the normal to the plane, from vertical is increased, the average nominal separation also increases, because the normal component of gravity, which causes the sphere to settle back toward the opposing surface after it is lifted away by a large asperity, is reduced.

The irreversible nature of particle–particle contacts, which are capable of compressive but not tensile forces, modifies suspension behaviour and rheology. For example, the resulting asymmetry in particle trajectories causes normal stress differences in sheared suspensions, at least for the roughness heights and solids concentrations examined, whereas the normal stress differences are absent for perfectly smooth spheres. It is also shown that microscopic surface roughness and particle–particle contacts generally lower the effective viscosity of flowing suspensions, as they reduce viscous dissipation due to near-contact lubrication stresses. For properties, such as normal stress differences and hydrodynamic diffusivities, that are sensitive to the separation between the nominal surfaces of the spheres at the position where two particles separate (i.e. where the compressive normal force pushing the particles together becomes zero), then the largest asperities are expected to play the dominant role, even if these large asperities are only sparsely distributed on the sphere surfaces.

This work was supported by the US National Science Foundation grant CTS-9712604 and the US National Aeronautics and Space Administration grant NCC3-796.

References

Batchelor, G. K. & Green, J. T. 1972*a* The determination of the bulk stress in a suspension of spherical particles to order c^2. *J. Fluid Mech.* **56**, 401–427.

Batchelor, G. K. & Green, J. T. 1972*b* The hydrodynamic interaction of two small freely-moving spheres in a linear flow field. *J. Fluid Mech.* **56**, 375–400.

Brady, J. F. & Bossis, G. 1988 Stokesian dynamics. *A. Rev. Fluid Mech.* **20**, 111–157.

Brady, J. F. & Vicic, M. 1995 Normal stresses in colloidal dispersions. *J. Rheol.* **39**, 545–566.

Carty, J. J. 1957 Resistance coefficients for spheres on a plane boundary. BSc thesis, Department of Civil and Sanitary Engineering, Massachusetts Institute of Technology, Cambridge, MA.

daCunha, F. R. & Hinch, E. J. 1996 Shear-induced dispersion in a dilute suspension of rough spheres. *J. Fluid Mech.* **309**, 211–223.

Davis, R. H. 1992 Effects of surface roughness on a sphere sedimenting through a dilute suspension of neutrally buoyant spheres. *Phys. Fluids* A **12**, 2607–2619.

Durlofsky, L., Brady, J. F. & Bossis, G. 1987 Dynamic simulation of hydrodynamically interacting particles. *J. Fluid Mech.* **180**, 21–89.

Einstein, A. 1906 Eine neue Bestimmung der Moleküledimensionen. *Annln Phys.* **19**, 289–306.

Galvin, K. P., Zhao, Y. & Davis, R. H. 2001 Time-averaged hydrodynamic roughness of a noncolloidal sphere in low Reynolds number motion down an inclined plane. *Phys. Fluids* **13**, 3108–3119.

Goldman, A. J., Cox, R. G. & Brenner, H. 1967 Slow viscous motion of a sphere parallel to a plane wall. I. Motion through a quiescent fluid. *Chem. Engng Sci.* **22**, 637–651.

Kim, S. & Karrila, S. J. 1991 *Microhydrodynamics: principles and selected applications*. Butterworth-Heinemann.

King, M. R. & Leighton, D. T. 1997 Measurement of the inertial lift on a moving sphere in contact with a plane wall in shear flow. *Phys. Fluids* **9**, 1248–1255.

Laun, H. M. 1994 Normal stresses in extremely shear thickening polymer dispersions. *J. Non-Newton. Fluid Mech.* **54**, 87–108.

Morris, J. F. & Katyal, B. 2002 Microstructure from simulated Brownian suspension flows at large shear rate. *Phys. Fluids* **14**, 1920–1937.

Parsi, F. & Gadala-Maria, F. 1987 Fore-and-aft symmetry in a concentrated suspension of solid spheres. *J. Rheol.* **31**, 725–732.

Persson, B. N. J. 1998 *Sliding friction: physical principles and applications*. Springer.

Phung, T. N., Brady, J. F. & Bossis, G. 1996 Stokesian dynamics simulation of Brownian suspensions. *J. Fluid Mech.* **313**, 181–207.

Prokunin, A. N. 1998 Spherical particle sedimentation along an inclined plane at small Reynolds numbers. *Fluid Dynam.* **23**, 573–579.

Rampall, I., Smart, J. R. & Leighton, D. T. 1997 The influence of roughness on the particle-pair distribution function of dilute suspensions of non-colloidal spheres in simple shear flow. *J. Fluid Mech.* **339**, 1–24.

Savage, S. B. 1998 Analyses of slow high-concentration flows of granular materials. *J. Fluid Mech.* **377**, 1–26.

Smart, J. R. & Leighton, D. T. 1989 Measurement of the hydrodynamic surface roughness of noncolloidal spheres. *Phys. Fluids* A **1**, 52–60.

Smart, J. R., Beimfohr, S. & Leighton, D. T. 1993 Measurement of the translational and rotational velocities of a noncolloidal sphere rolling down a smooth inclined plane at low Reynolds number. *Phys. Fluids* A **5**, 13–24.

Tabatabaian, M. & Cox, R. G. 1991 Effect of contact forces on sedimenting spheres in Stokes flow. *Int. J. Multiph. Flow* **17**, 395–413.

Wilson, H. J. & Davis, R. H. 2000 The viscosity of a dilute suspension of rough spheres. *J. Fluid Mech.* **421**, 339–367.

Wilson, H. J. & Davis, R. H. 2002 Shear stress of a monolayer of rough spheres. *J. Fluid Mech.* **452**, 425–441.

Zeng, S., Kerns, E. T. & Davis, R. H. 1996 The nature of particle contacts in sedimentation. *Phys. Fluids* **8**, 1389–1396.

Zhao, Y. & Davis, R. H. 2002 Interaction of two touching spheres in a viscous fluid. *Chem. Engng Sci.* **57**, 1997–2006.

Zhao, Y. & Davis, R. H. 2003 Interaction of sedimenting spheres with multiple surface roughness scales. (Submitted.)

Zhao, Y., Galvin, K. P. & Davis, R. H. 2002 Motion of a sphere down a rough plane in a viscous fluid. *Int. J. Multiph. Flow* **28**, 1787–1800.